ELSEVIER

Journal of Molecular Structure: THEOCHEM 774 (2006) 1–6

THEO CHEM

www.elsevier.com/locate/theochem

Theoretical study of the intramolecular hydrogen bonds of aromatic peroxy radicals from OH–toluene reactions

Mingqiang Huang *, Weijun Zhang, Yong yang, Zhenya Wang, Liqing Hao, Wenwu Zhao, Weixiong Zhao, Jinsong Li, Xiaoming Gao

Anhui Institute of Optics and Fine Mechanics, Chinese Academy of Sciences, Hefei 230031, PR China

Received 1 April 2006; received in revised form 6 June 2006; accepted 14 June 2006
Available online 27 June 2006

Abstract

Three methyl-hydroxycyclohexadienyl peroxy radicals with intramolecular H-bonds were studied at B3LYP/6-31G(d), B3LYP/6-311+G(d,p) and B3LYP/6-311++G(2d,2p) levels, respectively. 2-hydroxy-1-methyl-cyclohexadienyl peroxy radical (II), 2-hydroxy-3-methyl-cyclohexadienyl peroxy radical (III), and 4-hydroxy-3-methyl-cyclohexadienyl peroxy radical (IV) exhibit red-shifted O–H···O H-bond. From the AIM analysis, it becomes evident that 2-hydroxy-3-methyl-cyclohexadienyl peroxy radical (III) intramolecularO–H···O H-bond is the strongest. This represents that 2-hydroxy-3-methyl-cyclohexadienyl peroxy radical (III) is the most stable isomer. It is clear that hydrogen bonding plays a role in stabilizing the peroxy radicals: the hydrogen bond lengths are 1.9804, 1.9566, and 2.4457 Å for (II), (III), and (IV), respectively, correlating with their relative stability. From the NBO analysis, it becomes evident that three red-shifted intramolecular H-bonds can be explained on the basis of the two opposite effects: hyperconjugation and rehybridization. The hyperconjugation is slightly dominant and overshadows the rehybridization in the O–H···O H-bond.

Keywords: Methyl-hydroxycyclohexadienyl peroxy radical; Red-shifted H-bond; AIM topological analysis; NBO analysis

1. Introduction

Toluene is the most abundant aromatic hydrocarbon in the atmosphere. Toluene molecules can easily be attacked by a reactive species, like hydroxyl radical OH, generating non-volatile and semi-volatile products which can result in secondary organic aerosol (SOA) formation through either a self-nucleation process or the gas/particle partitioning on the preexisting particulate matter [1]. Over the last two decades, experimental studies on the formation mechanism of SOA from photooxidation of toluene [2–5], and on the identification of their oxidation products [1,6–13] have been conducted in some laboratories over the world. Typically, ring opening products are the major products in the toluene photooxidation [1,6,7,9,10,12].

Until recently, it was believed that the toluene–OH reaction proceeded by both abstraction and addition pathways. The addition pathway, occurring 90% of the time, is the more prevalent route [14]. As Shown in Fig. 1, under atmospheric conditions, the OH–toluene adduct reacts with O_2 either by O_2 addition to form peroxy radicals or by H-abstraction to yield phenolic compounds. The latter channel has been shown to be relatively minor, accounting for about 16% of the total products. The fate of the peroxy radicals is governed by competition between reaction with NO to form alkoxy radicals and cyclization to form bicyclic radicals. The bicyclic radicals can undergo unimolecular rearrangement to form epoxide radicals or bimolecular reaction with O_2 to form bicyclic peroxy radicals. Given the steric hindrance problems associated with another cyclization, the bicyclic peroxy radicals react with NO to form a bicyclic oxy radicals and NO_2. The only path for the resulting bicyclic oxy radicals is fragmentation via favorable

* Corresponding author. Tel.: +86 551 5593174; fax: +86 551 5591551.
E-mail address: huangmingqiang@gmail.com (M. Huang).

0166-1280/$ - see front matter © 2006 Elsevier B.V. All rights reserved.
doi:10.1016/j.theochem.2006.06.021

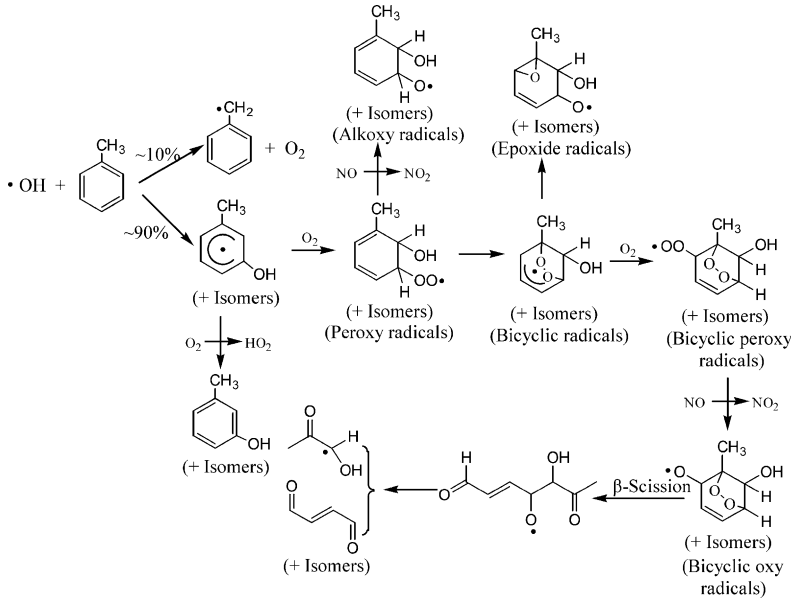

Fig. 1. Mechanistic diagram for the OH-initiated atmospheric photooxidation of toluene.

β-scission reactions. These fragmentation reactions yield an acyclic radical and eventually dicarbonyl products [3,5]. So, the fragmentation products are dependent on the peroxy radicals. And the peroxy radicals are the important intermediates in the toluene–OH reaction. In 2003, Suh et al. [5], reported a theoretical study of the aromatic peroxy, bicyclic, epoxide, and bicyclic peroxy radicals from the OH–toluene reactions. They found that there exists intramolecular hydrogen bonding in the peroxy radicals. It involves interaction between the terminal oxygen of the peroxy group and the hydrogen of the OH group, forming a six-membered ring. However, they only simply mentioned there exists intramolecular O–H···O H-bond in the peroxy radicals, they did not further confirm the existence of the H-bond and discuss the origin of the H-bond.

To the best of our knowledge, no investigations on the interesting intramolecular H-bond in the methyl-hydroxycyclohexadienyl peroxy radicals are performed up to now. Because of the complex picture of the possible pathways branching from toluene, the present theoretical investigation is focused on purpose only part of them. As the lowest energy toluene–OH adduct is 2-methyl-hydroxycyclohexadienyl radical (I), that resulting from OH addition to the ortho position. Namely, this paper will deal with those intramolecular H-bonds that initiate from the radical (I), generated by O_2 addition to radical (I). The main purpose of the work is to confirm the existence of the H-bond by AIM topological analysis and discuss the origin of the red-shifted H-bond by NBO analysis.

2. Computational methods

To obtain accurate energetic and rovibrational data, the structures and harmonic vibration frequencies of the 2-methyl-hydroxycyclohexadienyl radical (I), O_2, 2-hydroxy-1-methyl-cyclohexadienyl peroxy radical (II), 2-hydroxy-3-methyl-cyclohexadienyl peroxy radical (III), and 4-hydroxy-3-methyl-cyclohexadienyl peroxy radical (IV) were studied using the B3LYP method with the 6-31G(d), 6-311+G (d,p) and 6-311++G(2d,2p) basis sets, respectively. The basis set superposition error (BSSE) was calculated according to the counterpoise method proposed by Boys and Bernardi [15]. We performed natural bond orbital (NBO) [16] calculations for the 2-methyl-hydroxycyclohexadienyl radical (I), O_2, and peroxy radicals at the B3LYP/6-311+G(d,p) level. Atoms in molecules (AIM) [17] analysis is also carried out at the B3LYP/6-311+G(d,p) level. All the calculations were performed using the Gaussian-98 program package [18].

3. Results and discussion

3.1. Geometries, frequencies, and energies

The structures of the 2-methyl-hydroxycyclohexadienyl radical (I), O_2, 2-hydroxy-1-methyl-cyclohexadienyl peroxy radical (II), 2-hydroxy-3-methyl-cyclohexadienyl peroxy radical (III), and 4-hydroxy-3-methyl-cyclohexadienyl peroxy radical (IV) are shown in Fig. 2. The geometric parameters calculated using the B3LYP/6-31G(d), B3LYP/6-311+G(d,p), and B3LYP/6-311++G(2d,2p) levels are listed in Table 1. As shown in Table 1, the results indicate that there is a good agreement between various levels. For peroxy radical (II), the calculated distance for O17···H19 is 1.9804 Å. It is worthy of mentioning that there is a O17–O16–C1–C6–O18–H19 six-membered ring in the peroxy radical (II). In the cyclic structure, O17–H19–O18 is not linear. From the Table 1, it can be seen that there is a large red shift (68 cm^{-1}) of the O18–H19 stretching frequency in the peroxy radical (II).

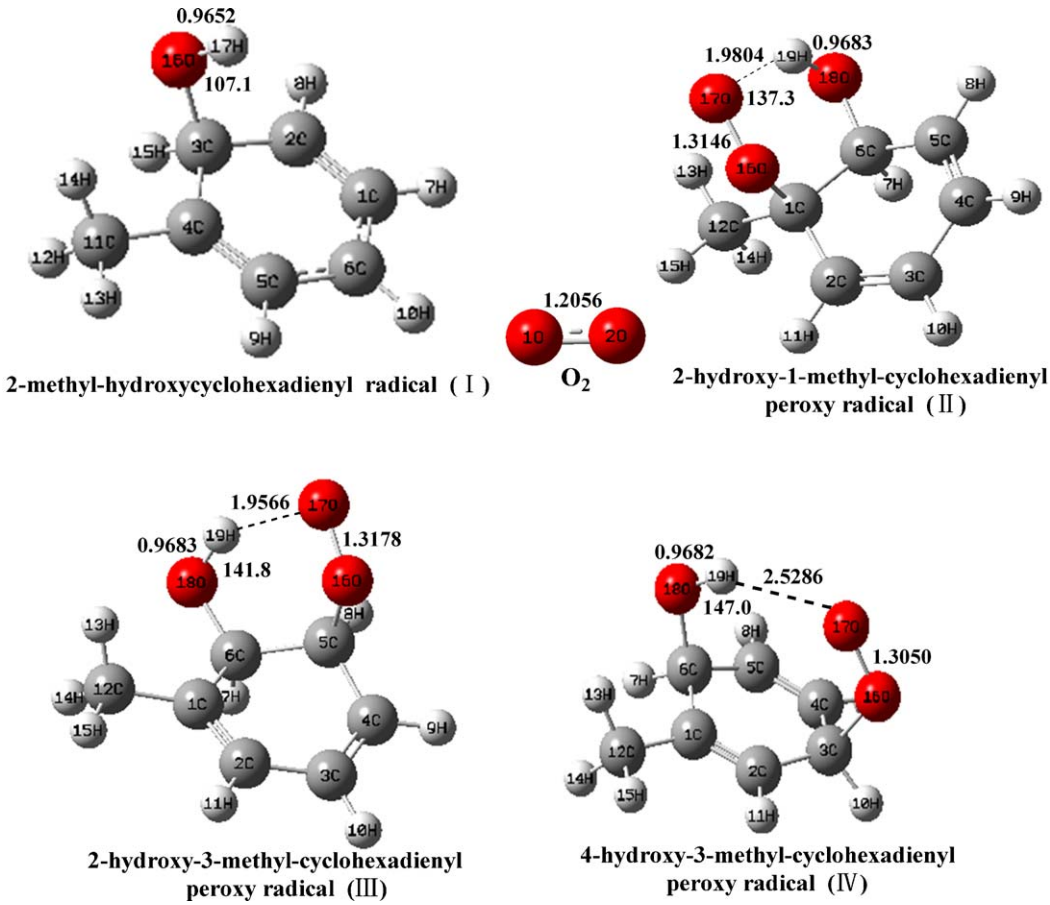

Fig. 2. Optimized geometries of the radical (I), O_2, peroxy radical (II), (III), and (IV) at the B3LYP/6-311+G(d,p) level bond lengths in (Å), bond angles in (°).

Table 1
The change of bond length, the change of bond stretching frequency and the interaction energy with BSSE correction at the B3LYP/6-31G(d), B3LYP/6-311+G(d,p), and B3LYP/6-311++G(2d,2p) levels

	B3LYP/6-31G(d)	B3LYP/6-311+G(d,p)	B3LYP/6-311++G(2d,2p)
Peroxy radical (II)			
Δr(O18–H19)/Å	+0.0036	+0.0031	+0.0034
Δv(O18–H19)/cm^{-1}	−69	−68	−76
ΔE^{BSSE}/kJ mol^{-1}	−17.98	−6.93	−7.70
Peroxy radical (III)[a]			
Δr(O18–H19)/Å	+0.0037	+0.0031	+0.0034
Δv(O18–H19)/cm^{-1}	−81	−81	−87
ΔE^{BSSE}/kJ mol^{-1}	−21.39	−10.70	−12.15
Peroxy radical (IV)			
Δr(O18–H19)/Å	+0.0039	+0.0030	+0.0024
Δv(O18–H19)/cm^{-1}	−48	−42	−34
ΔE^{BSSE}/kJ mol^{-1}	−13.20	−5.21	−5.34

[a] For peroxy radical (III), the interaction energy with BSSE correction also determined at MP2/6-31+G(d) level. It is −48.19 kJ/mol, which is larger than that get by B3LYP method. This is because, contrast to most ab initio methods, and Møller-Plesset in particular, B3LYP is known to underestimate the height of reaction barriers (see text).

This frequency shift correlates with the bond elongation (0.0031 Å) of the O18–H19 bond.

The structure of the peroxy radical (III) is similar to that of peroxy radical (II). The corresponding length for O17···H19 is 1.9566 Å in the peroxy radical (III) at the B3LYP/6-311+G(d,p) level. There is also a O17–O16–C5–C6–O18–H19 six-membered ring in the peroxy radical (II). In the cyclic structure, O17–H19–O18 is not linear. Peroxy radical (III) exhibits a red shift (81 cm^{-1}) of the O18–H19 stretching frequency, and this frequency shift also correlates with the bond elongation (0.0031 Å) of the O18–H19 bond.

The corresponding length for O17···H19 is 2.5286 Å in the peroxy radical (IV) at the B3LYP/6-311+G(d,p) level. Peroxy radical (IV) exhibits a red shift (42 cm^{-1}) of the O18–H19 stretching frequency, and this frequency shift also correlates with the bond elongation (0.0032 Å) of the O18–H19 bond.

As shown in the Table 1, the interaction energies with BSSE correction for the peroxy radicals (II), (III), and (IV) are −6.93, −10.70, and −5.21 kJ mol^{-1} at the B3LYP/6-311+G(d,p) level, respectively. The results show that the peroxy radical (III) is the most stable in the 3 peroxy radicals. For accurate description of hydrogen-bonded system, we also use MP2/6-31+G(d) to determine interaction energy with BSSE correction for peroxy radical (III). It is −48.19 kJ/mol, which is larger than that get by B3LYP method. This is because, contrast to most ab initio methods, and MØller-Plesset in particular, B3LYP is known to underestimate the height of reaction barriers [19]. In fact, as García-Cruz et al. [20] had noted, in several cases, that MP2 method consistently emphasizes the positive interactions in compounds where additions occurs on the substituted carbon atom on the ring. Moreover, MP2 method is impractical at this time due to the large size of the hydroxy-methylcyclohexadienyl peroxy radicals molecule and the need for an open-shell treatment. However, B3LYP density functional method has already been validated in earlier studies on open-shell systems [5,21–26], For these systems, B3LYP results differed on average less than 1 kcal/mol from high-level ab initio calculations, and most often reproduced experimental barriers heights within 0.5 kcal/mol. Hence, we believe the B3LYP density functional method to be in general a reliable method for the calculations presented here.

3.2. AIM topological analysis

To confirm the existence of the red-shifted intermolecular H-bond, we performed "Atoms In Molecules (AIM)" topological analysis. Popelier and colleagues [27,28] proposed a set of criteria for the existence of H-Bond, among which three are most often applied [29]. The electron density and its Laplacian for the H···Y contact within the X–H···Y H-bond should have a relatively high value. Both parameters for opened-shell interactions as H-bond are positive and should be within the following ranges: 0.002–0.035 a.u. for the electron density and 0.024–0.139 a.u. for its Laplacian. According to the topological analysis of the electron density in the theory of AIM, ρ is used to describe the strength of a bond. In general, the larger the value of ρ is, the stronger the bond is. The $\nabla^2\rho$ describes the characteristic of the bond. Where $\nabla^2\rho < 0$, the bond is covalent bond, as $\nabla^2\rho > 0$, the bond belongs to the ionic bond, hydrogen bond, and van der Waals interactions. Here, $\nabla^2\rho = \lambda_1 + \lambda_2 + \lambda_3$, λ_i is an eigenvalue of the Hessian matrix of ρ. Then, when one of the three λ_i is positive and the other two are negative, we denote it by $(3,-1)$ and call it the bond critical point (BCP). As shown in Table 2, the value of the electron density ρ for O17···H19 in the peroxy radicals (II), (III), and (IV) are 0.0254, 0.0259, and 0.0078 a.u. These values do fall within the proposed typical range of the H-bond. Since the ρ(O17···H19) in the peroxy radical (III) is the largest, we expect the O–H···O bond in the peroxy radical (III) to be the strongest. This represents that 2-hydroxy-3-methyl-cyclohexadienyl peroxy radical (III) is the most stable isomer. It is clear that hydrogen bonding plays a role in stabilizing the peroxy radicals: the hydrogen bond lengths are 1.9804, 1.9566, and 2.4457 Å for (II), (III), and (IV), respectively, correlating with their relative stability. The values of the $\nabla^2\rho$ for O17···H19 in the peroxy radicals (II), (III), and (IV) are 0.0897, 0.0921, and 0.0237 a.u., respectively. These values are also in the range of the H-bond.

On the basis of the AIM topological analysis, we have proved that the O–H···O bond can be classified as H-bonds in the peroxy radicals (II), (III), and (IV). It should be pointed out that the O–H bond in the peroxy radicals (II), (III), and (IV) exhibit red shift. However, the AIM analysis does not reveal the origin of the red-shifted H-bonds. This problem was solved by performing the natural bond orbital (NBO) analysis.

3.3. NBO analysis

It is clear from Fig. 2 that the H-bonds are complicated in the peroxy radicals (II), (III), and (IV). The peroxy radicals (II), (III), and (IV) exhibit red-shifted O–H···O. To interpret and explain the nature of the above-mentioned red-shifted H-bonds, we performed the NBO analysis for the peroxy radicals (II), (III), and (IV). The results are presented in Tables 3 and 4.

In the NBO analysis, the importance of hyperconjugative interaction and electron density transfer (EDT) from lone electron pairs of the Y atom to the X–H antibonding orbital in the X–H···Y system is well-documented [16]. In general, such interactions lead to an increase in the population of X–H antibonding orbital. The increase of the electron density in X–H antibonding orbital weakens the X–H bond, which leads to its elongation and concomitant red

Table 2
Topological parameters of the bond critical point at the B3LYP/6-311+G(d,p) level

	BCP	ρ	$\nabla^2\rho$	λ_1	λ_2	λ_3	ϵ
Peroxy radical (II)	O17–H19	0.0254	0.0897	−0.0336	−0.0320	0.1553	0.0495
Peroxy radical (III)	O17–H19	0.0259	0.0921	−0.0349	−0.0332	0.1602	0.0514
Peroxy radical (IV)	O17–H19	0.0078	0.0237	−0.0069	−0.0068	0.0375	0.0182

Table 3
The energy of hyperconjugative interaction ($kJ\,mol^{-1}$) and occupancy (e) at the B3LYP/6-311+G(d,p) level

$E^{(2)}$	Monomers	Peroxy radical (II)	Peroxy radical (III)	Peroxy radical (IV)
n_1(O17) → σ^* (O18–H19)	–	7.64	3.82	1.13
n_2(O17) → σ^* (O18–H19)	–	–	8.02	–
Occupancy				
σ^* (O18-H19)	0.00352	0.01213	0.01251	0.00594
n_1(O17)	0.99901	0.99391	0.99416	0.99717
n_2(O17)	0.99901	0.97659	0.97937	0.97147

Table 4
The natural atomic charges (e), hybridization and polarization at the B3LYP/6-311+G(d,p) level

	Monomers	Peroxy radical (II)	Peroxy radical (III)	Peroxy radical (IV)
q(O17)	0.50000	−0.43016	−0.43013	0.25183
q(O18)	−0.39693	−0.37296	−0.37585	−0.36465
q(H19)	0.22890	0.24137	0.24291	0.23704
spn(O18–19)	sp 3.69	sp 3.39	sp 3.26	sp 3.68
% s-char	21.31%	22.73%	23.44%	21.36%
pol O18%	73.38%	75.05%	75.25%	74.20%
($\sigma_{O18–H19}$), H19%	26.62%	24.95%	24.75%	25.80%

shift of the X–H stretching frequency. Furthermore, Alabugin et al. [30] recently showed that structural reorganization of X–H bond in the process of both blue-shifted and red-shifted H-bonds was determined by the balance of the opposing effects: X–H bond lengthening effect due to hyperconjugative $n(Y) \rightarrow \sigma^*$ (X–H) interaction and X–H bond shortening effect due to rehybridization. On the basis of the theoretical model, it should not be difficult to explain the red shift of O–H bond stretching frequency in the peroxy radicals (II), (III), and (IV).

For the O18–H19···O17 H-bond in the peroxy radicals (II), (III), and (IV), Table 3 shows that the hyperconjugative $n_1(O17) \rightarrow \sigma^*$ (O18–H19) interactions are relatively significant. The corresponding increase of electron density in the σ^* (O18–H19) weakens and elongates the O18–H19 bond, which results in the red shift of the O18–H19 bond stretching frequency. In contrast, according to the rehybridization model, the O18–H19···O17 H-bond formation increases O18–H19 bond polarization and positive charge on H19 atom. These changes results in a simultaneous increase in the s-character in the O18 hybrid orbital of O18–H19 bond. Table 4 shows that the s-character of the O18–H19 bond in the O18–H19···O17 H-bond increases from $sp^{3.69}$ to $sp^{3.26}$ which strengthens the O18–H19 bond. Because hyperconjugation and rehybridization act in opposite directions, the red shift and blue shift of the bond O18–H19 is a result of a balance of two effects. And for O18–H19···O17 H-bonds in the peroxy radicals (II), (III), and (IV), the hyperconjugative $n(O17) \rightarrow \sigma^*$ (O18–H19) interaction is beyond the 21 $kJ\,mol^{-1}$ threshold, which indicates that the hyperconjugation is very important. So, the fact is simple: the hyperconjugation is dominant and overshadows the rehybridization in the O18–H19···O17 H-bond. To this point, the NBO results fully explain the observations of the red shift of the O18–H19 stretching frequency in the peroxy radicals (II), (III), and (IV).

4. Conclusion

Three methyl-hydroxycyclohexadienyl peroxy radicals, 2-hydroxy-1-methyl-cyclohexadienyl peroxy radical (II), 2-hydroxy-3-methyl-cyclohexadienyl peroxy radical (III), and 4-hydroxy-3-methyl-cyclohexadienyl peroxy radical (IV) exhibit red-shifted O–H···O H-bond. From the AIM analysis, it becomes evident that 2-hydroxy-3-methyl-cyclohexadienyl peroxy radical (III) intramolecular O–H···O H-bond is the strongest. This explains why that 2-hydroxy-3-methyl-cyclohexadienyl peroxy radical (III) is the most stable isomer. From the NBO analysis, it becomes evident that three red-shifted intramolecular H-bonds can be explained on the basis of the two opposite effects: hyperconjugation and rehybridization. The hyperconjugation is slightly dominant and overshadows the rehybridization in the H-bond. We conclude that hydrogen bonding plays a role in stabilizing the methyl-hydroxycyclohexadienyl peroxy radicals.

Acknowledgements

This work is supported by National Natural Science Foundation of China (20477043) and Knowledge Innovation Foundation of Chinese Academy of Sciences (KJCX2-SW-H08). The authors express our gratitude to the referees for their value comments.

References

[1] M.S. Jang, R.M. Kamens, Environ. Sci. Technol. 35 (2001) 3626.
[2] L.J. Bartolotti, E.O. Edney, Chem. Phys. Lett. 245 (1995) 119.
[3] J.M. Andino, J.N. Smith, R.C. Flagan, W.A. Goddard, J.H. Seinfeld, J. Phys. Chem. 100 (1996) 10967.
[4] I. Suh, D. Zhang, R.Y. Zhang, L.T. Molina, M.J. Molina, Chem. Phys. Lett. 364 (2002) 454.

[5] I. Suh, R.Y. Zhang, L.T. Molina, M.J. Molina, J. Am. Chem. Soc. 125 (2003) 12655.
[6] P.B. Shepson, E.O. Edeny, E.W. Corse, J. Phys. Chem. 88 (1984) 4122.
[7] E.C. Tuazon, R. Atkinson, H.M. Leod, H.W. Blermann, A.M. Winer, W.P.L. Carter Jr., Environ. Sci. Technol. 18 (1984) 981.
[8] R. Atkinson, S.M. Aschmann, J. Arey, W.P.L. Carter, Int. J. Chem. Kinet. 21 (1991) 801.
[9] H.J.L. Forstner, R.C. Flagan, J.H. Seinfeld, Environ. Sci. Technol. 31 (1997) 1345.
[10] J. Yu, H.E. Jeffries, K.G. Sexton, Atmos. Environ. 31 (1997) 2261.
[11] J. Yu, H.E. Jeffries, Atmos. Environ. 31 (1997) 2281.
[12] D.F. Smith, C.D. McIver, T.E. Kleindienst, J. Atmos. Chem. 30 (1998) 209.
[13] M.J. Molina, R. Zhang, K. Broekhuizen, W. Lei, R. Navarro, L.T. Molina, J. Am. Chem. Soc. 121 (1999) 10225.
[14] R. Atkinson, Atmos. Environ. 34 (2000) 2063.
[15] S.F. Boys, F. Bernardi, Mol. Phys. 19 (1970) 553.
[16] A.E. Reed, L.A. Curtiss, F. Weinhold, Chem. Rev. 88 (1988) 899.
[17] R.F.W. Bader, Atoms in Molecules: A Quantum Theory, Oxford University Press, Oxford, 1990.
[18] M.J. Frisch, G.W. Trucks, H.B. Schlegel, G.E. Scuseria, M.A. Robb, J.R. Cheeseman, V.G. Zakrzewski, J.A. Montgomery Jr., R.E. Stratmann, J.C. Burant, S. Dapprich, J.M. Millam, A.D. Daniels, K.N. Kudin, M.C. Strain, O. Farkas, J. Tomasi, V. Barone, M. CossiR. Cammi, B. Mennucci, C. Pomelli, C. Adamo, S. Clifford, J. Ochterski, G.A. Petersson, P.Y. Ayala, Q. Cui, K. Morokuma, D.K. Malick, A.D. Rabuck, K. Raghavachari, J.B. Foresman, J. Cioslowski, J.V. Ortiz, A.G. Baboul, B.B. Stefanov, G. Liu, A. Liashenko, P. Piskorz, I. Komaromo, R. Gomperts, R.L. Martin, D.J. Fox, T. Keith, M.A. Allaham, C.Y. Peng, A. Nanayakkara, C. Gonzalez, M. Challacombe, P.M.W. Gill, B. Johnson, W. Chen, M.M. Wong, J.L. Andres, C. Gonzalez, M. Head-Gordon, E.S. Replogle, J.A. Pople, Gaussian 98, Revision A. 7, Gaussian, Inc., Pittsburgh PA, 1998.
[19] I. García-Cruz, M.E. Rui'z-Santoyo, J.R. Alvarez-Idaboy, A. Vivier-Bunge, J. Comput. Chem. 20 (1999) 845.
[20] I. García-Cruz, M. Castro, A. Vivier-Bunge, J. Comput. Chem. 21 (2000) 716.
[21] L. Vereecken, K. Pierloot, J. Peeters, J. Chem. Phys. 108 (1998) 1068.
[22] J.J. Orlando, G.S. Tyndall, M. Bilde, C. Ferronato, T.J. Wallington, L. Vereecken, J. Peeters, J. Phys. Chem. A 102 (1998) 8116.
[23] L. Vereecken, J. Peeters, J. Phys. Chem. A 103 (1999) 1768.
[24] L. Vereecken, J. Peeters, J.J. Orlando, G.S. Tyndall, C. Ferronato, J. Phys. Chem. A 103 (1999) 4693.
[25] L. Vereecken, J. Peeters, J. Phys. Chem. A 104 (2000) 11140.
[26] W. Lei, R. Zhang, J. Phys. Chem. A 105 (2001) 3808.
[27] U. Kock, P.L.A. Popelier, J. Phys. Chem. A 99 (1995) 9747.
[28] P.L.A. Popelier, J. Phys. Chem. A 102 (1998) 1873.
[29] P. Lipkowski, S.J. Grabowski, T.L. Robinson, J. Leszczynski, J. Phys. Chem. A 108 (2004) 10865.
[30] I.V. Alabugin, M. Manoharan, S. Peabody, F. Weinhold, J. Am. Chem. Soc. 125 (2003) 5973.